

Article

Hierarchical NiCo₂O₄ Hollow Sphere as a Peroxidase Mimetic for Colorimetric Detection of H₂O₂ and Glucose

Wei Huang ¹, Tianye Lin ¹, Yang Cao ¹, Xiaoyong Lai ², Juan Peng ² and Jinchun Tu ^{1,*}

¹ State Key Laboratory of Marine Resource Utilization in South China Sea, Key Laboratory of Tropical Biological Resources of Ministry of Education Hainan University, College of Material and Chemical Engineering, Haikou 570228, China; hw_hnu@aliyun.com (W.H.); HDxuchufeng@163.com (T.L.); cy507@hainu.edu.cn (Y.C.)

² Laboratory Cultivation Base of Natural Gas Conversion, School of Chemistry and Chemical Engineering, Ningxia University, Yinchuan 750021, China; xylai@nxu.edu.cn (X.L.); pengjuan@nxu.edu.cn (J.P.)

* Correspondence: tujinchun@hainu.edu.cn; Tel./Fax: +86-898-6625-9764

Academic Editors: Jong Seung Kim and Min Hee Lee

Received: 6 December 2016; Accepted: 16 January 2017; Published: 23 January 2017

Abstract: In this work, the hierarchical NiCo₂O₄ hollow sphere synthesized via a “coordinating etching and precipitating” process was demonstrated to exhibit intrinsic peroxidase-like activity. The peroxidase-like activity of NiCo₂O₄, NiO, and Co₃O₄ hollow spheres were comparatively studied by the catalytic oxidation reaction of 3,3,5,5-tetramethylbenzidine (TMB) in presence of H₂O₂, and a superior peroxidase-like activity of NiCo₂O₄ was confirmed by stronger absorbance at 652 nm. Furthermore, the proposed sensing platform showed commendable response to H₂O₂ with a linear range from 10 μM to 400 μM, and a detection limit of 0.21 μM. Cooperated with GOx, the developed novel colorimetric and visual glucose-sensing platform exhibited high selectivity, favorable reproducibility, satisfactory applicability, wide linear range (from 0.1 mM to 4.5 mM), and a low detection limit of 5.31 μM. In addition, the concentration-dependent color change would offer a better and handier way for detection of H₂O₂ and glucose by naked eye.

Keywords: NiCo₂O₄; hierarchical hollow sphere; peroxidase-like; colorimetric

1. Introduction

Natural enzymes have been widely studied and applied in various fields due to their high substrate specificity and brilliant catalytic activity under mild conditions [1]. However, application of these enzymes is restricted by their high cost, complicated purification and immobilization procedures, and harsh reaction conditions [2,3]. Therefore, the low-cost enzyme mimics with good stability, excellent catalytic activity, and satisfactory selectivity were highly in demand [4]. Since Gao’s [5] first report on an intrinsic peroxidase-like activity of Fe₃O₄ nanoparticles, various nanomaterials such as MFe₂O₄ [6,7], MoS₂ [8], Co₃O₄ [9,10], NiO [11], CuS [12], graphene oxide [13], and graphene oxide–Fe₃O₄ composite [14] have been further investigated as peroxidase mimetics for H₂O₂ detection. These researches reveal that the nanomaterial-based peroxidase mimetics possess the advantages of high specific surface area, controllable morphologies and sizes, and tunable catalytic properties that would be promising candidates for bioassays and clinical diagnosis [4,15,16].

NiCo₂O₄ is a typical spinal metal oxide, with Ni ions occupying the octahedral sites while Co ions are integrally distributed to both the octahedral and tetrahedral sites [17,18]. Due to its superior catalytic activity and conductivity to that of single Co₃O₄ or NiO [19,20], NiCo₂O₄ has gained great attention in the areas of supercapacitor, electrocatalyst, oxidation evolution reaction, and biosensor [21,22]. It has been reported that Co₃O₄ nanoparticles possess an intrinsic peroxidase-like

and catalase-like activity, and NiO exhibits peroxidase-like activity as well [9,11,23]. The surface of NiCo_2O_4 is rich in oxidation states $\text{Ni}^{2+}/\text{Ni}^{3+}$ and $\text{Co}^{2+}/\text{Co}^{3+}$, which make it a better electron transfer mediator for peroxidase substrates (such as 3,3,5,5-tetramethylbenzidine (TMB)) and H_2O_2 analysis. Moreover, the superior conductivity of NiCo_2O_4 is conducive to improving the electron transfer kinetics within the materials. To the best of our knowledge, the study of NiCo_2O_4 as an enzyme mimetic remains unexplored, which greatly inspires the research interest in applying nanostructured NiCo_2O_4 to colorimetric detection of H_2O_2 . Besides, it is well known that the catalytic properties of active materials seriously depend on their morphology and size, which significantly influence the surface efficiency and stability of catalysts [24,25]. The hierarchical hollow structure assembled from particle units is endowed with the advantages of high surface-to-volume ratio, ample mass diffusion pathways, and satisfactory structure stability [26,27]. Therefore, the hierarchical hollow structured NiCo_2O_4 materials are expected to function as highly efficient peroxidase mimetics for colorimetric detection of H_2O_2 and glucose.

In this paper, the hierarchical NiCo_2O_4 hollow sphere was prepared through a facile Cu_2O -templated approach based on the “coordinating etching and precipitating” (CEP) process, and its peroxidase-like activity was investigated for the first time. Moreover, the peroxidase-like activity of the hierarchical NiCo_2O_4 hollow sphere was compared to that of single NiO and Co_3O_4 with the presence of TMB and H_2O_2 under parallel condition. In addition, the hierarchical NiCo_2O_4 hollow sphere was applied to the colorimetric detection of H_2O_2 . Combined with glucose oxidase (GOx), a novel colorimetric and visual glucose-sensing platform was developed. Finally, the selectivity, reproducibility, and applicability of this proposed sensing platform were assessed by a standard method.

2. Experimental

2.1. Chemicals

$\text{CuCl}_2 \cdot 2\text{H}_2\text{O}$, sodium dodecyl sulfate (SDS), NaOH, $\text{NH}_2\text{OH} \cdot \text{HCl}$, $\text{CoCl}_2 \cdot 6\text{H}_2\text{O}$, $\text{Na}_2\text{S}_2\text{O}_3 \cdot 5\text{H}_2\text{O}$, glucose, and absolute ethanol were purchased from Shanghai Sinopharm Chemical Reagent Co., Ltd. (Shanghai, China). Polyvinylpyrrolidone (PVP, K30, MW \approx 3800) was provided by Aldrich (Shanghai, China). Citric acid monohydrate, trisodium citrate dihydrate, and 30% H_2O_2 were supplied by Guangzhou Chemical Reagent Factory ich (Guangzhou, China). TMB was obtained from Macklin ich (Shanghai, China). Glucose oxidase (GOx, 50 KU) was procured from Sangon Biotech (Shanghai, China) Co., Ltd. (Shanghai, China) and stored in a freezer at -20°C . All chemical reagents were of analytical grade and were used without further purification.

2.2. Apparatus

X-ray diffraction (XRD) analysis was performed using a D8 Tools XRD instrument (Bruker, Karlsruhe, Germany) with a voltage of 40 kV and a current of 30 mA with Cu $\text{K}\alpha$ radiation ($k = 1.5406 \text{ \AA}$). Field-emission scanning electron microscope (SEM) images were obtained by Hitachi S-4800. Transmission electron microscopy (TEM) micrographs were acquired using a JEOL-2100F microscope. The ζ -potential was measured using dynamic light scattering (DLS) at 25°C (Malvern Nanosizer ZS90). X-ray photoelectron spectroscopy (XPS) data were characterized by Thermo Scientific ESCALAB250 (Thermo Scientific, Waltham, MA, USA) using Al radiation. Nitrogen sorption experiments were carried out at 77 K on a Micro Meritics Tristar II 3020 surface area and pore size analyzer (Norcross, GA, USA). Prior to the measurements, the samples were outgassed at 200°C in vacuum for 6 h. UV-vis absorption spectra were recorded using a 723PC spectrophotometer (Shanghai Jinghua Science and Technology Co., Ltd., Shanghai, China).

2.3. Synthesis of Hierarchical NiCo_2O_4 Hollow Sphere

The NiCo_2O_4 hollow sphere was synthesized based on a “CEP” process by selecting $\text{S}_2\text{O}_3^{2-}$ as etchant towards the pre-prepared Cu_2O solid-sphere template. The Cu_2O solid sphere was obtained

according to our previous work [28]. First, 5 mg of the as-prepared Cu₂O nanospheres, 1.13 mg of CoCl₂·6H₂O, 0.57 mg of NiCl₂·6H₂O, and 0.33 g of PVP were dissolved into a mixed solution ($V_{\text{ethanol}}:V_{\text{water}} = 1:1$, 10 mL), stirred, and sonicated. Then, 4 mL of Na₂S₂O₃ aqueous solution (1 M) was added dropwise into the mixture and kept stirring for about 10 min. The resulting precursor was collected by several rinse–centrifugation cycles with deionized (DI) water and ethanol. Finally, the precursor was calcinated in a muffle furnace at 300 °C for 4 h at a ramp rate of 1 °C·min⁻¹ under the air condition.

2.4. Catalytic Oxidation of TMB

To investigate the peroxidase-like activity of NiCo₂O₄ hollow sphere, catalytic oxidation reaction of TMB in sodium citrate buffer solution was performed in presence of H₂O₂. Five microliters of 1 mg·mL⁻¹ NiCo₂O₄ hollow sphere dispersion was incubated with 3 mL of pre-prepared sodium citrate buffer solution (0.1 M, pH 4.5) in the presence of H₂O₂ (0.02 M) and TMB (0.08 mM). The photographs and UV-vis spectra were obtained after incubation at room temperature for 30 min.

2.5. Colorimetric Detection of H₂O₂

Five microliters of 1 mg/mL NiCo₂O₄ hollow sphere dispersion, 25 μL of 10 mM TMB, and 3 μL of H₂O₂ in different concentrations were added to 3 mL sodium citrate buffer solution (0.1 M, pH 4.5). The UV-vis absorption spectra were recorded from 500 nm to 800 nm.

2.6. Colorimetric Detection of Glucose

Five microliters of 1 mg/mL NiCo₂O₄ hollow sphere dispersion, 25 μL of 10 mM TMB, 5 μL of 10 mg/mL GOx, and 3 μL of glucose in different concentrations were added to 3 mL of sodium citrate buffer solution (0.1 M, pH 4.5). The UV-vis absorption spectra were recorded from 500 nm to 800 nm.

3. Results and Discussion

3.1. Materials Characterization

The Ni–Co hydroxide precursor was synthesized via a deliberately designed “CEP” process, and the duplication and the elimination of Cu₂O template were completed simultaneously within 10 min at room temperature [29,30]. The final NiCo₂O₄ hollow sphere product was obtained after a simple thermal treatment based on the above processes. As shown in Figure 1a, a high-quality Cu₂O template with an average size of approximately 400 nm was obtained, and its rough texture on the surface was conducive to creating more chemical etching interface. From the TEM image in Figure 1b, a solid construction can be confirmed. After the etching process and thermal treatment, the obtained NiCo₂O₄ sphere (Figure 1c) well inherited the spherical structure of the template, indicating the controllability of the “CEP” process and the stability in structure. The “wormlike” secondary structures can be observed clearly in the magnified image in Figure 1d, and the hollow structure feature can be initially identified by the cracked sphere. Afterwards, we performed TEM characterization to further testify to the inner structure of the hierarchical sphere.

As shown in Figure 2a,b, the distinct contrast between the shells and inner space fully demonstrates the hollow construction of the hierarchical NiCo₂O₄ sphere. The diameter of the hollow sphere is about 400 nm, which is similar to that of pre-grown Cu₂O sphere. Furthermore, the apparent bright and dark aberrations on the ultrathin shell (<30 nm) imply the existence of nanopores, and sheetlike secondary structures of several nanometers in thickness are uniformly grown on the sphere. Notably, the ultrathin hollow sphere with affluent secondary structures could provide more efficient inner and outer surface and create more catalytically active sites. The inserted selected area electron diffraction (SAED) pattern in Figure 2b reveals a polycrystalline feature of the as-prepared material. Figure 2c displays the amplified image of the selected area marked in (b), in which the nanopore and ripple structure can be identified, and the high-resolution TEM image in Figure 2d also

attests to the evident crystalline structure in the NiCo_2O_4 hollow sphere. More detailed structure information was further determined by XRD and N_2 adsorption–desorption tests.

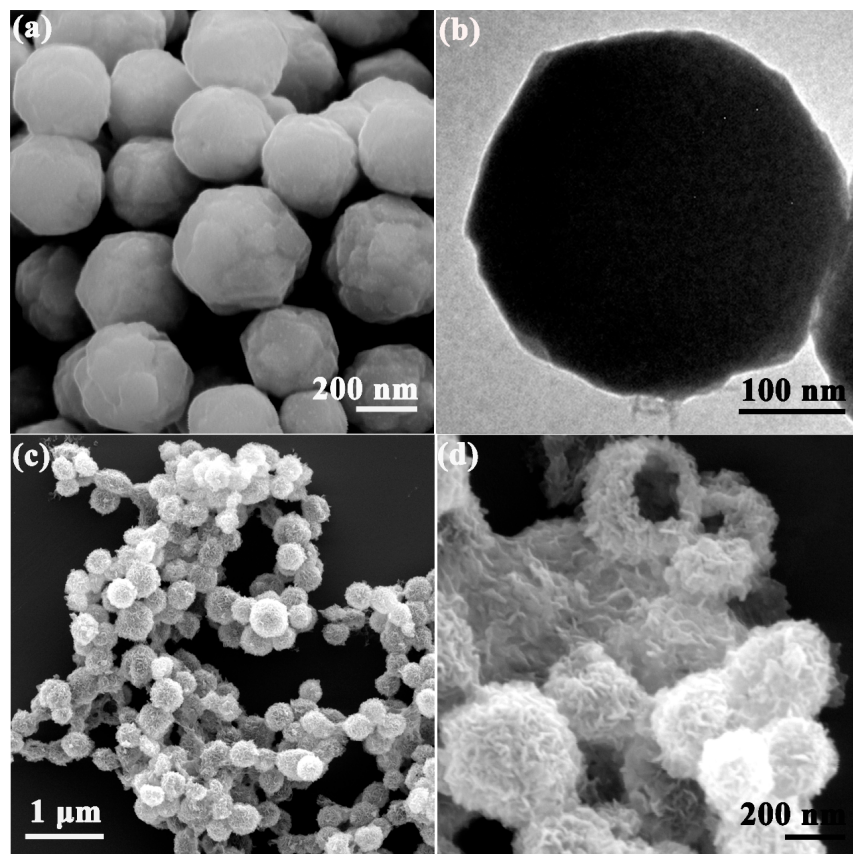


Figure 1. (a,b) SEM and TEM images of Cu_2O solid sphere; (c,d) SEM images of the hierarchical NiCo_2O_4 hollow sphere.

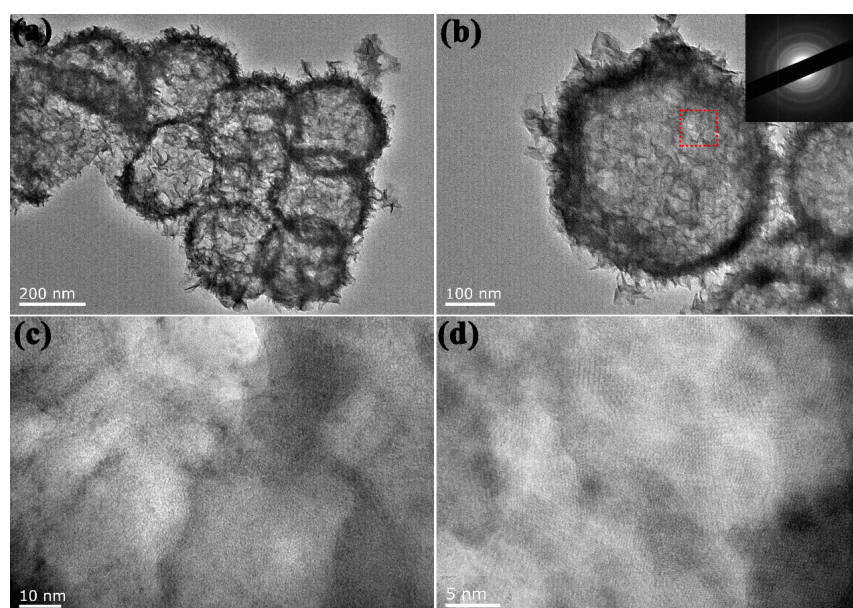


Figure 2. TEM (a–c) and HRTEM (d) images of NiCo_2O_4 hollow sphere. Inset in (b) is the corresponding selected area electron diffraction (SAED) pattern.

Figure 3a depicts the typical XRD pattern of the as-prepared materials, in which all diffraction peaks can be assigned to the spinal-structured NiCo_2O_4 (JCPDS No. 20-0781). The peaks at 2θ values of 31° , 36° , 45° , 59° , and 65° are corresponding to (200), (311), (400), (511), and (440) crystal faces of NiCo_2O_4 in cubic phase [31]. No other impurity peaks appear, indicating the high purity of the samples. The porosity of the hierarchical NiCo_2O_4 hollow sphere was assessed by N_2 adsorption–desorption test as shown in Figure 3b, which gives a typical IV-type isotherm. The specific surface area estimated by Brunauer–Emmett–Teller (BET) method is $59.4 \text{ m}^2 \cdot \text{g}^{-1}$, and the inserted pore size distribution curve demonstrates the existence of mesopores [32]. Apparently, the porous structure of the hierarchical NiCo_2O_4 hollow sphere is beneficial to supply more mass transport pathways and active sites. Furthermore, the DLS result shows that the surface of the as-obtained NiCo_2O_4 hollow spheres is positively charged (about 3.0 mV) in water, which is conducive to the absorption of negatively charged GOx and improves the dispersibility of the particles in the solution. Additionally, the surface composition and valence state of the hierarchical NiCo_2O_4 hollow sphere are also vital, since the catalytic reactions mainly happened on the surface of catalysts.

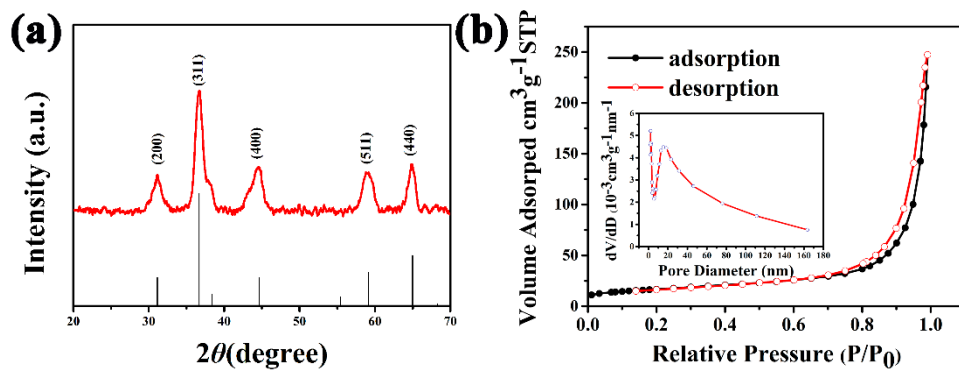


Figure 3. (a) X-ray diffraction (XRD) pattern of as-prepared NiCo_2O_4 hollow sphere sample; (b) N_2 adsorption–desorption isotherms, and inset is the corresponding pore size distribution of the as-prepared hierarchical NiCo_2O_4 hollow sphere.

XPS was applied to study the element and valance information of NiCo_2O_4 hollow sphere. The survey spectrum in Figure 4a demonstrates the existence of nickel, cobalt, oxygen, and slight carbon atoms. By using a Gaussian fitting, the high-resolution spectrum of Ni 2p exhibits two spin-orbit doublets (Ni^{2+} and Ni^{3+}) and two shakeup satellites (Figure 4b). The peaks at 854.2 eV and 871.9 eV are attributed to Ni^{2+} , and the peaks at 855.8 eV and 873.5 eV can be assigned to Ni^{3+} . The Co 2p spectrum can also be fitted into two spin-orbit doublets (Co^{2+} and Co^{3+}) and two shakeup satellites (Figure 4c) in the same way. These results are well in agreement with many other reports, demonstrating the Ni^{2+} and Ni^{3+} , Co^{2+} and Co^{3+} inside the NiCo_2O_4 hollow sphere [33]. The high-resolution spectrum of O 1s exhibits three oxygen species marked as O1, O2, and O3. Based on the previous reports, O1 (with a binding energy of 529.5 eV) was a typical metal–oxygen bond, and O2 (with a binding energy of 530.7 eV) was generally attributed to defects, impurities, and some low oxygen coordination within the spinal structure [34]. As for O3 (with a binding energy of 531.6 eV), it was associated with physi- and chemisorbed water molecules [35]. The rich surface chemical composition and valence state of the NiCo_2O_4 hollow sphere may lead to a large number of distributional differences in local electronic cloud density, which greatly affect the catalytic activity.

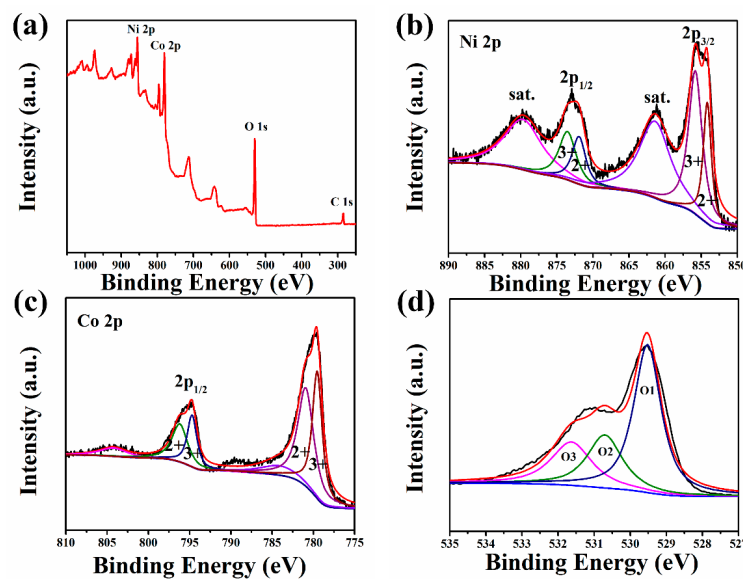


Figure 4. X-ray photoelectron spectroscopy (XPS) spectrum of the NiCo_2O_4 hollow sphere: (a) survey; (b) Ni 2p; (c) Co 2p; (d) O 1s.

3.2. Synthesis Mechanism

Based on the above discussion, the well-designed “CEP” process has been successfully applied to the synthesis of the hierarchical porous NiCo_2O_4 hollow sphere. Figure 5a–d display the evolution in morphology and structure, from Cu_2O solid sphere to the final hierarchical NiCo_2O_4 hollow sphere. Figure 5e displays the corresponding schematic illustration of the formation process. As is well known, according to the HSAB (hard and soft acids and bases) theory, Cu^+ has much stronger interaction with $\text{S}_2\text{O}_3^{2-}$ (soft–soft interaction) than that of O^{2-} (soft–hard interaction). Thus, the presence of $\text{S}_2\text{O}_3^{2-}$ would lead to the elimination of the Cu_2O template and an increased local OH^- concentration on the etching interface. Besides, accompanied by the hydrolyzation of $\text{S}_2\text{O}_3^{2-}$ and coprecipitation of metal ions with OH^- , Ni–Co hydroxide units are preferential to nucleation and growth at the etching interface to form the Ni–Co hydroxide hollow sphere (Figure 5b). It is noteworthy that both the template elimination and duplication processes can be accurately controlled by simply adjusting the ratio of water to ethanol.

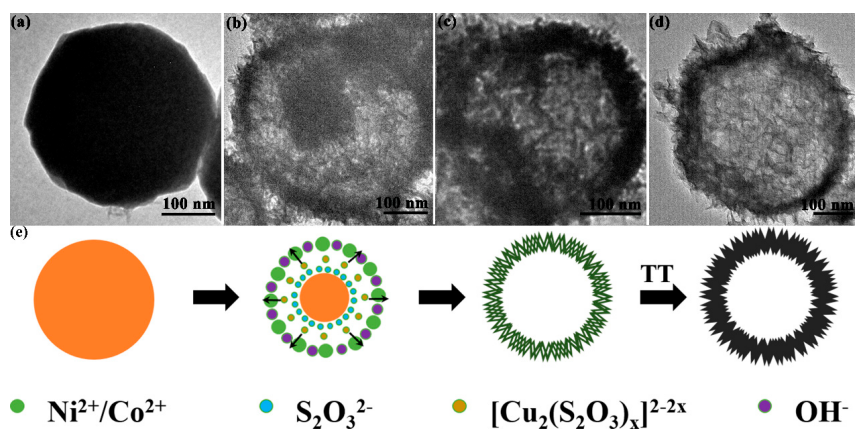


Figure 5. Representative TEM images of the samples at different stages: (a) Cu_2O ; (b) $\text{Cu}_2\text{O}@\text{Ni–Co}$ hydroxide; (c) Ni–Co hydroxide hollow sphere precursor; and (d) NiCo_2O_4 hollow sphere. (e) The corresponding schematic illustration of the formation process for hierarchical NiCo_2O_4 hollow sphere. Abbreviations: TT, thermal treatment.

3.3. Peroxidase-Like Activity of the Hierarchical NiCo₂O₄ Hollow Sphere

To investigate the peroxidase-like activity of the hierarchical NiCo₂O₄ hollow sphere, the catalysis of the peroxidase substrate TMB was performed in presence or absence of H₂O₂. Additionally, the peroxidase-like activities of NiO and Co₃O₄ hollow spheres synthesized by the same method were also studied for comparison. Thus, five controlled experiments were carried out: (i) TMB + H₂O₂; (ii) TMB + NiCo₂O₄; (iii) TMB + H₂O₂ + NiCo₂O₄; (iv) TMB + H₂O₂ + NiO; (v) TMB + H₂O₂ + Co₃O₄. As shown in Figure 6a, only with the coexistence of H₂O₂ and NiCo₂O₄ catalyst could beget an obvious absorption peak at 652 nm (iii) due to the oxidation of TMB, which indicates a peroxidase-like activity. As in previous reported work, both of the as-prepared NiO (iv) and Co₃O₄ (v) catalysts exhibited peroxidase-like activity in this research. However, the corresponding absorption spectra reveals that the hierarchical NiCo₂O₄ hollow sphere obviously possesses a stronger absorption peak than that of NiO and Co₃O₄ under the parallel condition, suggesting an enhanced peroxidase-like activity. The possible reaction mechanism is different from that of Fe-based catalysts, which are mainly conducted by the “Fenton” reaction. During this process, TMB molecules are absorbed on the surface of the hierarchical NiCo₂O₄ hollow sphere, and can donate lone-pair electrons from the amino groups to the catalyst [8]. That results in an increase in electron density and mobility in the NiCo₂O₄ hollow sphere, which would facilitate the electron transfer from the NiCo₂O₄ hollow sphere to H₂O₂ to accelerate the oxidation rate of TMB by H₂O₂ [9]. Furthermore, the enhanced peroxidase-like activity of the NiCo₂O₄ catalyst should be attributed to the diversified distribution of surface electron clouds and the hierarchical porous hollow structure that could provide ample active sites for catalytic reaction. The peroxidase-like activity of the hierarchical NiCo₂O₄ hollow sphere is also dependent on the TMB concentration and pH environment. As shown in Figure 6b, the absorption intensity at 652 nm was increased with the increasing of TMB, but no obvious increase was observed when the concentration was greater than 0.08 mM (25 μL), suggesting an optimized TMB concentration. Additionally, the pH-dependent peroxidase-like activity in Figure 6c indicates that the optimal pH should be 4.5.

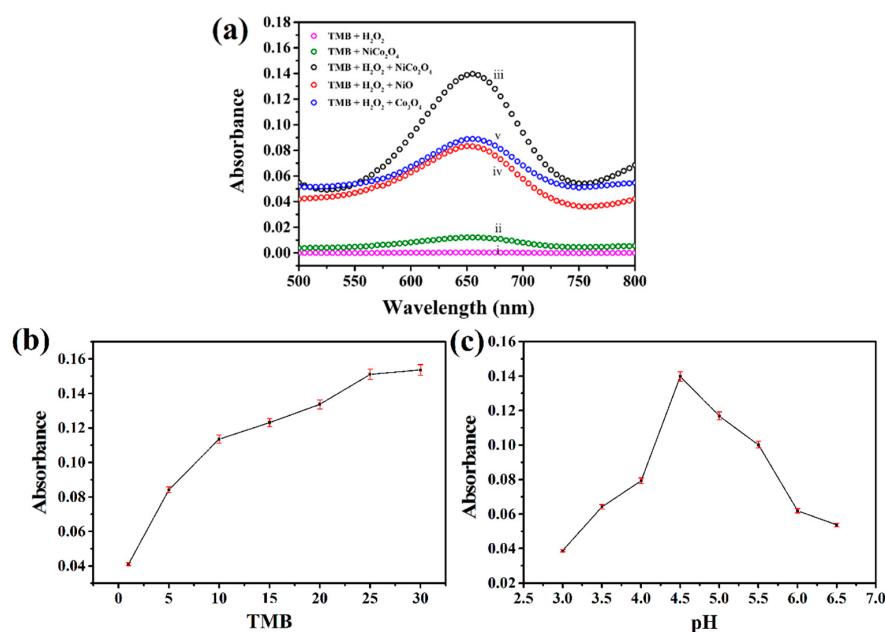


Figure 6. (a) Photograph and absorption spectra of colorimetric reactions under different conditions: (i) 3,3,5,5-tetramethylbenzidine (TMB) + H₂O₂; (ii) TMB + NiCo₂O₄; (iii) TMB + H₂O₂ + NiCo₂O₄; (iv) TMB + H₂O₂ + NiO; (v) TMB + H₂O₂ + Co₃O₄. TMB concentration- (b) and pH- (c) dependent peroxidase-like activity of hierarchical NiCo₂O₄ hollow sphere. Experimental conditions: 5 μL of 1 mg·mL⁻¹ enzyme mimetic dispersions were incubated with 3 mL of pre-prepared sodium citrate buffer solution (0.1 M, pH 4.5) with the presence of H₂O₂ (0.02 M) and TMB (0.08 mM).

3.4. Colorimetric Detection of H_2O_2

Based on the above peroxidase-like activity investigation of the hierarchical $NiCo_2O_4$ hollow sphere, a colorimetric method was developed for detection of H_2O_2 . In Figure 7a, the absorbance at 652 nm for oxidized TMB increases with the concentration of H_2O_2 . Figure 7b shows the corresponding linear calibration curve and photograph of color change. The linear range is from 0.01 mM to 0.4 mM, and the detection limit is calculated to be 0.21 μ M. Notably, the concentration-dependent color change could offer a handy way for detection of H_2O_2 by naked eye.

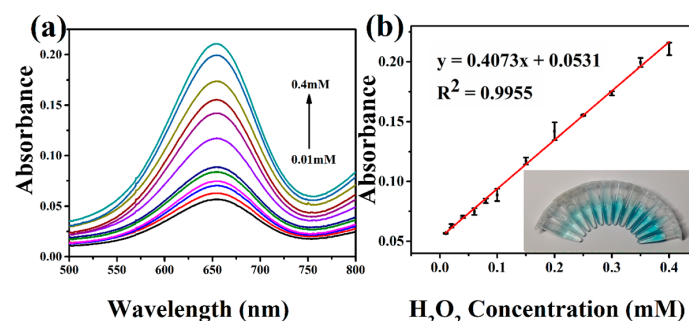


Figure 7. (a) Absorption spectra of the hierarchical $NiCo_2O_4$ hollow sphere with various concentrations of H_2O_2 (0.01–0.4 mM). (b) The corresponding linear calibration curve. The inset shows the photograph of color change for various concentrations.

3.5. Colorimetric Detection of Glucose

The concentration of blood glucose is an important physiological indicator for the human body. The detection of glucose is meaningful for clinical diagnosis and treatment of disease. H_2O_2 is one of the main intermediate products of glucose oxidase-catalyzed reaction. To take full advantage of the peroxidase-like activity of the hierarchical $NiCo_2O_4$ hollow sphere, the colorimetric detection of glucose was also developed, and the reaction mechanism is illustrated in Figure 8. As shown in Figure 9a, the absorbance at 652 nm for oxidized TMB increases with the concentration of H_2O_2 . The corresponding linear calibration curve and photograph of color change in Figure 9b shows that the linear range is from 0.1 mM to 4.5 mM with a detection limit of 5.31 μ M. It can be seen from Table 1 that the proposed catalyst performs satisfactory combination properties toward glucose sensing compared with most non-Pt-based catalysts. Even though the present $NiCo_2O_4$ -based sensor exhibits slightly lower sensing performance to that of a Pt-based sensor, but it is also a low-cost and effective detection method. Moreover, the concentrations of blood glucose in healthy and diabetic persons is generally in the range of 3–8 mM and 9–40 mM, respectively [36]. Therefore, the proposed method is applicable to glucose analysis in real serum by simple dilution.

Table 1. Comparison of the linear ranges and the detection limits with other methods for the detection of glucose.

Catalyst	Linear Range (μ M)	Detection Limit (μ M)	Reference
$NiCo_2O_4$	100–4500	5.31	This work
CuO	100–8000	-	[37]
V_2O_5	10–2000	10	[3]
Au nanoparticles	30–1000	30	[38]
FeCPNPs	2–20	1	[39]
$H_2TCPP-Co_3O_4$ nanocomposites	1–10	0.86	[40]
Zn^{2+} /AMP nanofiber	-	0.6	[41]
CeO_2 nanoparticle	-	8.9	[42]
Pt-DNA complexes	0.1–1000	0.1	[43]

FeCPNPs: Fe (III)-based coordination polymer nanoparticles. H_2TCPP : 5,10,15,20-Tetrakis(4-carboxyl phenyl)-porphyrin. AMP: Adenosine 5'-monophosphate.

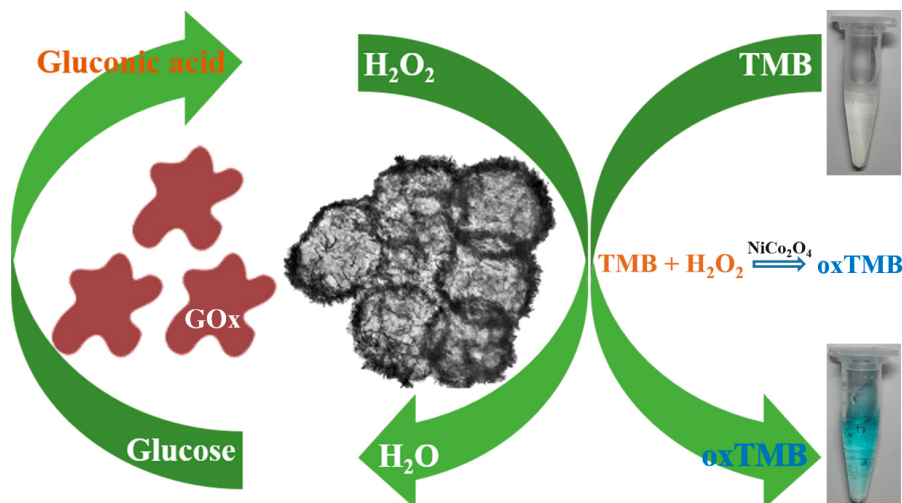


Figure 8. Scheme illustration for colorimetric detection of glucose using the hierarchical NiCo₂O₄ hollow sphere.

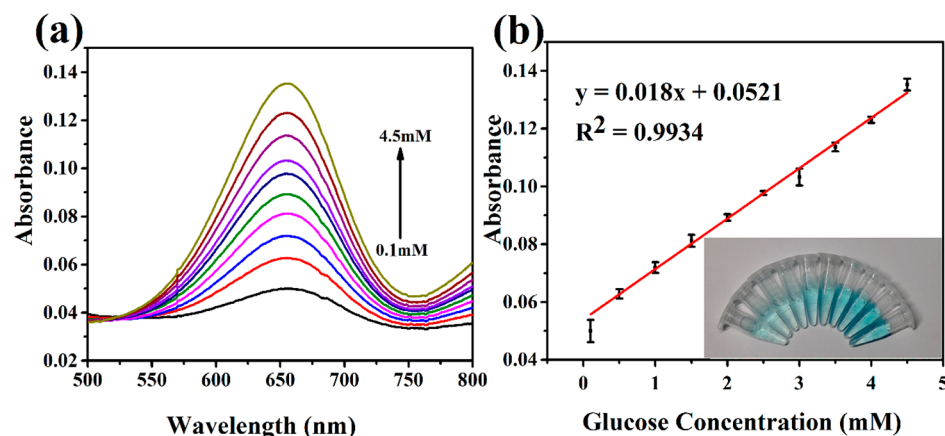


Figure 9. (a) Absorption spectra of the hierarchical NiCo₂O₄ hollow sphere with various concentrations of glucose (0.1–4.5 mM). (b) The corresponding linear calibration curve. The inset shows the photograph of color change for various concentrations.

3.6. Selectivity, Reproducibility, and Applicability

The selectivity, reproducibility, and applicability of the proposed sensor for glucose detection were investigated. As shown in Figure 10, the presence of glucose apparently produced much stronger absorption intensity and color change than that of other analytes, indicating a good selectivity to glucose of this biosensor. The reproducibility was evaluated by three consecutive detections, resulting in an acceptable relative standard deviation (RSD) of 3.24%. For applicability, the sensor was applied to detect the human serum sample: the detected glucose concentration was 4.2 mM with an acceptable RSD of 4.5%, compared to the concentration of 4.4 mM determined by the hospital.

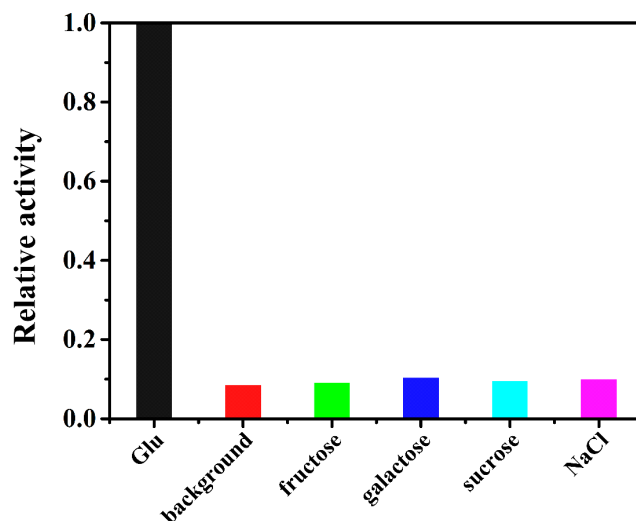


Figure 10. Selectivity of the proposed sensor for glucose detection was assessed by measuring the absorption intensity at 652 nm. The concentrations for fructose, galactose, sucrose, and NaCl are 20 mM, respectively.

4. Conclusions

In summary, the hierarchical NiCo_2O_4 hollow sphere was successfully synthesized by a “coordinating etching and precipitating” process and exhibited intrinsic peroxidase-like activity. The experimental results revealed that the hierarchical NiCo_2O_4 hollow sphere possessed superior peroxidase-like activity to that of single NiO or Co_3O_4 . For use as a peroxidase mimic, the proposed sensing platform showed a commendable response to H_2O_2 with a linear range from 10 μM to 400 μM and a detection limit of 0.21 μM . More importantly, combined with GOx, the developed glucose-sensing platform exhibited high selectivity, superb reproducibility, satisfactory applicability, wide linear range from 0.1 mM to 4.5 mM, and low detection limit of 5.31 μM . Additionally, the concentration-dependent color change could offer a handy way for detection of H_2O_2 and glucose by naked eye. Therefore, the hierarchical NiCo_2O_4 hollow sphere would be a promising candidate for colorimetric detection of H_2O_2 and glucose.

Acknowledgments: This research was financially supported by National Natural Science Foundation of China (No. 21301042 and 51361009) and National Basic Research Program of China (973 program, No. 2012CB9339020).

Author Contributions: Jinchun Tu conceived and designed the experiments; Wei Huang performed the experiments and analyzed the data; Jinchun Tu contributed reagents/materials/analysis tools; Wei Huang, Tianye Lin, Yang Cao, Xiaoyong Lai, Juan Peng and Jinchun Tu wrote the paper.

Conflicts of Interest: The authors declare no conflict of interest. The funding sponsors had no role in the design of the study; in the collection, analyses, or interpretation of data; in the writing of the manuscript, and in the decision to publish the results.

References

- Bankar, S.B.; Bule, M.V.; Singhal, R.S.; Ananthanarayan, L. Glucose oxidase—An overview. *Biotechnol. Adv.* **2009**, *27*, 489–501. [[CrossRef](#)] [[PubMed](#)]
- Ronkainen, N.J.; Halsall, H.B.; Heineman, W.R. Electrochemical biosensors. *Chem. Soc. Rev.* **2010**, *39*, 1747–1763. [[CrossRef](#)] [[PubMed](#)]
- Sun, J.; Li, C.; Qi, Y.; Guo, S.; Liang, X. Optimizing Colorimetric Assay Based on V_2O_5 Nanozymes for Sensitive Detection of H_2O_2 and Glucose. *Sensors* **2016**, *16*, 584. [[CrossRef](#)] [[PubMed](#)]
- Kuah, E.; Toh, S.; Yee, J.; Ma, Q.; Gao, Z. Enzyme Mimics: Advances and Applications. *Chem. Eur. J.* **2016**, *22*, 8404–8430. [[CrossRef](#)] [[PubMed](#)]

5. Gao, L.; Zhuang, J.; Nie, L.; Zhang, J.; Zhang, Y.; Gu, N.; Wang, T.; Feng, J.; Yang, D.; Perrett, S.; et al. Intrinsic peroxidase-like activity of ferromagnetic nanoparticles. *Nat. Nanotechnol.* **2007**, *2*, 577–583. [[CrossRef](#)] [[PubMed](#)]
6. Su, L.; Qin, W.; Zhang, H.; Rahman, Z.U.; Ren, C.; Ma, S.; Chen, X. The peroxidase/catalase-like activities of MFe₂O₄ (M = Mg, Ni, Cu) MNPs and their application in colorimetric biosensing of glucose. *Biosens. Bioelectron.* **2015**, *63*, 384–391. [[CrossRef](#)] [[PubMed](#)]
7. Su, L.; Feng, J.; Zhou, X.; Ren, C.; Li, H.; Chen, X. Colorimetric Detection of Urine Glucose Based ZnFe₂O₄ Magnetic Nanoparticles. *Anal. Chem.* **2012**, *84*, 5753–5758. [[CrossRef](#)] [[PubMed](#)]
8. Zhao, K.; Gu, W.; Zheng, S.; Zhang, C.; Xian, Y. SDS–MoS₂ nanoparticles as highly-efficient peroxidase mimetics for colorimetric detection of H₂O₂ and glucose. *Talanta* **2015**, *141*, 47–52. [[CrossRef](#)] [[PubMed](#)]
9. Mu, J.; Wang, Y.; Zhao, M.; Zhang, L. Intrinsic peroxidase-like activity and catalase-like activity of Co₃O₄ nanoparticles. *Chem. Commun.* **2012**, *48*, 2540–2542. [[CrossRef](#)] [[PubMed](#)]
10. Zhang, Z.; Hao, J.; Yang, W.; Lu, B.; Ke, X.; Zhang, B.; Tang, J. Porous Co₃O₄ Nanorods-Reduced Graphene Oxide with Intrinsic Peroxidase-Like Activity and Catalysis in the Degradation of Methylene Blue. *ACS Appl. Mater. Interfaces* **2013**, *5*, 3809–3815. [[CrossRef](#)] [[PubMed](#)]
11. Ray, C.; Dutta, S.; Sarkar, S.; Sahoo, R.; Roy, A.; Pal, T. Intrinsic peroxidase-like activity of mesoporous nickel oxide for selective cysteine sensing. *J. Mater. Chem. B* **2014**, *2*, 6097–6105. [[CrossRef](#)]
12. Dutta, A.K.; Das, S.; Samanta, S.; Samanta, P.K.; Adhikary, B.; Biswas, P. CuS nanoparticles as a mimic peroxidase for colorimetric estimation of human blood glucose level. *Talanta* **2013**, *107*, 361–367. [[CrossRef](#)] [[PubMed](#)]
13. Song, Y.; Qu, K.; Zhao, C.; Ren, J.; Qu, X. Graphene Oxide: Intrinsic Peroxidase Catalytic Activity and Its Application to Glucose Detection. *Adv. Mater.* **2010**, *22*, 2206–2210. [[CrossRef](#)] [[PubMed](#)]
14. Dong, Y.-L.; Zhang, H.-G.; Rahman, Z.U.; Su, L.; Chen, X.-J.; Hu, J.; Chen, X.-G. Graphene oxide-Fe₃O₄ magnetic nanocomposites with peroxidase-like activity for colorimetric detection of glucose. *Nanoscale* **2012**, *4*, 3969–3976. [[CrossRef](#)] [[PubMed](#)]
15. Ragg, R.; Tahir, M.N.; Tremel, W. Solids Go Bio: Inorganic Nanoparticles as Enzyme Mimics. *Eur. J. Inorg. Chem.* **2016**, *2016*, 1906–1915. [[CrossRef](#)]
16. Liu, B.; Han, X.; Liu, J. Iron oxide nanozyme catalyzed synthesis of fluorescent polydopamine for light-up Zn²⁺ detection. *Nanoscale* **2016**, *8*, 13620–13626. [[CrossRef](#)] [[PubMed](#)]
17. Verma, S.; Joshi, H.M.; Jagadale, T.; Chawla, A.; Chandra, R.; Ogale, S. Nearly Monodispersed Multifunctional NiCo₂O₄ Spinel Nanoparticles: Magnetism, Infrared Transparency, and Radiofrequency Absorption. *J. Phys. Chem. C* **2008**, *112*, 15106–15112. [[CrossRef](#)]
18. Knop, O.; Reid, K.I.G.; Sutarno; Nakagawa, Y. Chalkogenides of the transition elements. VI. X-ray, neutron, and magnetic investigation of the spinels Co₃O₄, NiCo₂O₄, Co₃S₄, and NiCo₂S₄. *Can. J. Chem.* **1968**, *46*, 3463–3476. [[CrossRef](#)]
19. Alcántara, R.; Jaraba, M.; Lavela, P.; Tirado, J.L. NiCo₂O₄ Spinel: First Report on a Transition Metal Oxide for the Negative Electrode of Sodium-Ion Batteries. *Chem. Mater.* **2002**, *14*, 2847–2848. [[CrossRef](#)]
20. Zhou, W.; Kong, D.; Jia, X.; Ding, C.; Cheng, C.; Wen, G. NiCo₂O₄ nanosheet supported hierarchical core-shell arrays for high-performance supercapacitors. *J. Mater. Chem. A* **2014**, *2*, 6310–6315. [[CrossRef](#)]
21. Hussain, M.; Ibupoto, Z.; Abbasi, M.; Liu, X.; Nur, O.; Willander, M. Synthesis of Three Dimensional Nickel Cobalt Oxide Nanoneedles on Nickel Foam, Their Characterization and Glucose Sensing Application. *Sensors* **2014**, *14*, 5415–5425. [[CrossRef](#)] [[PubMed](#)]
22. Jadhav, H.S.; Kalubarme, R.S.; Park, C.-N.; Kim, J.; Park, C.-J. Facile and cost effective synthesis of mesoporous spinel NiCo₂O₄ as an anode for high lithium storage capacity. *Nanoscale* **2014**, *6*, 10071–10076. [[CrossRef](#)] [[PubMed](#)]
23. Jia, H.; Yang, D.; Han, X.; Cai, J.; Liu, H.; He, W. Peroxidase-like activity of the Co₃O₄ nanoparticles used for biodetection and evaluation of antioxidant behavior. *Nanoscale* **2016**, *8*, 5938–5945. [[CrossRef](#)] [[PubMed](#)]
24. Burch, R. Gold catalysts for pure hydrogen production in the water-gas shift reaction: Activity, structure and reaction mechanism. *Phys. Chem. Chem. Phys.* **2006**, *8*, 5483–5500. [[CrossRef](#)] [[PubMed](#)]
25. Gong, J. Structure and Surface Chemistry of Gold-Based Model Catalysts. *Chem. Rev.* **2012**, *112*, 2987–3054. [[CrossRef](#)] [[PubMed](#)]
26. Zhao, Y.; Jiang, L. Hollow Micro/Nanomaterials with Multilevel Interior Structures. *Adv. Mater.* **2009**, *21*, 3621–3638. [[CrossRef](#)]

27. Hu, J.; Chen, M.; Fang, X.; Wu, L. Fabrication and application of inorganic hollow spheres. *Chem. Soc. Rev.* **2011**, *40*, 5472–5491. [CrossRef] [PubMed]
28. Xu, C.F.; Cao, Y.; Chen, Y.; Huang, W.; Chen, D.L.; Huang, Q.Y.; Tu, J.C. Fast Synthesis of Hierarchical Co(OH)₂ Nanosheet Hollow Spheres with Enhanced Glucose Sensing. *Eur. J. Inorg. Chem.* **2016**, *2016*, 3163–3168. [CrossRef]
29. Nai, J.; Tian, Y.; Guan, X.; Guo, L. Pearson’s Principle Inspired Generalized Strategy for the Fabrication of Metal Hydroxide and Oxide Nanocages. *J. Am. Chem. Soc.* **2013**, *135*, 16082–16091. [CrossRef] [PubMed]
30. Wang, Z.; Luan, D.; Boey, F.Y.C.; Lou, X.W. Fast Formation of SnO₂ Nanoboxes with Enhanced Lithium Storage Capability. *J. Am. Chem. Soc.* **2011**, *133*, 4738–4741. [CrossRef] [PubMed]
31. Ma, F.-X.; Yu, L.; Xu, C.-Y.; Lou, X.W. Self-supported formation of hierarchical NiCo₂O₄ tetragonal microtubes with enhanced electrochemical properties. *Energy Environ. Sci.* **2016**, *9*, 862–866. [CrossRef]
32. Zhang, Y.; Ma, M.; Yang, J.; Su, H.; Huang, W.; Dong, X. Selective synthesis of hierarchical mesoporous spinel NiCo₂O₄ for high-performance supercapacitors. *Nanoscale* **2014**, *6*, 4303–4308. [CrossRef] [PubMed]
33. Liu, L.; Wang, J.; Hou, Y.; Chen, J.; Liu, H.-K.; Wang, J.; Wu, Y. Self-Assembled 3D Foam-Like NiCo₂O₄ as Efficient Catalyst for Lithium Oxygen Batteries. *Small* **2016**, *12*, 602–611. [CrossRef] [PubMed]
34. Liu, L.; Zhang, H.; Yang, J.; Mu, Y.; Wang, Y. Self-assembled novel dandelion-like NiCo₂O₄ microspheres@nanomeshes with superior electrochemical performance for supercapacitors and lithium-ion batteries. *J. Mater. Chem. A* **2015**, *3*, 22393–22403. [CrossRef]
35. Yu, X.; Sun, Z.; Yan, Z.; Xiang, B.; Liu, X.; Du, P. Direct growth of porous crystalline NiCo₂O₄ nanowire arrays on a conductive electrode for high-performance electrocatalytic water oxidation. *J. Mater. Chem. A* **2014**, *2*, 20823–20831. [CrossRef]
36. Jiang, H.; Chen, Z.; Cao, H.; Huang, Y. Peroxidase-like activity of chitosan stabilized silver nanoparticles for visual and colorimetric detection of glucose. *Analyst* **2012**, *137*, 5560–5564. [CrossRef] [PubMed]
37. Chen, W.; Chen, J.; Feng, Y.-B.; Hong, L.; Chen, Q.-Y.; Wu, L.-F.; Lin, X.-H.; Xia, X.-H. Peroxidase-like activity of water-soluble cupric oxide nanoparticles and its analytical application for detection of hydrogen peroxide and glucose. *Analyst* **2012**, *137*, 1706–1712. [CrossRef] [PubMed]
38. Xu, X.; Yang, X. Facile colorimetric detection of glucose based on an organic Fenton reaction. *Anal. Methods* **2011**, *3*, 1056–1059. [CrossRef]
39. Tian, J.; Liu, S.; Luo, Y.; Sun, X. Fe(III)-based coordination polymer nanoparticles: Peroxidase-like catalytic activity and their application to hydrogen peroxide and glucose detection. *Catal. Sci. Technol.* **2012**, *2*, 432–436. [CrossRef]
40. Liu, Q.; Zhu, R.; Du, H.; Li, H.; Yang, Y.; Jia, Q.; Bian, B. Higher catalytic activity of porphyrin functionalized Co₃O₄ nanostructures for visual and colorimetric detection of H₂O₂ and glucose. *Mater. Sci. Eng. C* **2014**, *43*, 321–329. [CrossRef] [PubMed]
41. Liang, H.; Jiang, S.; Yuan, Q.; Li, G.; Wang, F.; Zhang, Z.; Liu, J. Co-immobilization of multiple enzymes by metal coordinated nucleotide hydrogel nanofibers: Improved stability and an enzyme cascade for glucose detection. *Nanoscale* **2016**, *8*, 6071–6078. [CrossRef] [PubMed]
42. Liu, B.; Sun, Z.; Huang, P.-J.J.; Liu, J. Hydrogen Peroxide Displacing DNA from Nanoceria: Mechanism and Detection of Glucose in Serum. *J. Am. Chem. Soc.* **2015**, *137*, 1290–1295. [CrossRef] [PubMed]
43. Chen, X.; Zhou, X.; Hu, J. Pt-DNA complexes as peroxidase mimetics and their applications in colorimetric detection of H₂O₂ and glucose. *Anal. Methods* **2012**, *4*, 2183–2187. [CrossRef]



© 2017 by the authors; licensee MDPI, Basel, Switzerland. This article is an open access article distributed under the terms and conditions of the Creative Commons Attribution (CC BY) license (<http://creativecommons.org/licenses/by/4.0/>).